Hindawi
International Transactions on Electrical Energy Systems
Volume 2024, Article ID 2794393, 16 pages
https://doi.org/10.1155/2024/2794393

Research Article

Calculation Method and Characteristic Analysis for Fault Current of Permanent Magnet Direct-Drive Wind Power System considering Positive and Negative Sequence Decomposition

Botong Li,[1,2] **Qing Zhong**,[1,2] **Weijie Wen**,[1,2] **Bin Li**,[1,2] **and Xiaolong Chen**[1,2]

[1]*Key Laboratory of Smart Grid of Minist of Education, Tianjin University, Tianjin 300072, China*
[2]*National Industry-Education Platform of Energy Storage, Tianjin University, Tianjin 300072, China*

Correspondence should be addressed to Weijie Wen; weijie.wen@tju.edu.cn

Received 4 May 2023; Revised 30 January 2024; Accepted 5 February 2024; Published 20 February 2024

Academic Editor: Mohammad Ashraf Hossain Sadi

In view of the fact that the influence of positive and negative sequence decomposition, which is widely used in positive and negative sequence decoupling control in control system, on the fault current calculation process is not deeply considered in the existing transient analysis methods of permanent magnet direct-drive wind farm short circuit current, this paper proposes a transient short circuit current calculation model that takes into account positive and negative sequence decomposition. The influence of the transient characteristics of positive and negative sequence decomposition on the control system is studied, and the mechanism of its action on the transient change of short circuit current is revealed. The positive and negative sequence decoupling processes of the circuit equation are modified, and the characteristics of the coupling equation are analyzed. The difference in the converter output voltage between the circuit equation and the control equation and the depth of its influence on the calculation process is revealed. On the basis of quantifying the difference at the converter output voltage, the circuit equation and the control equation are combined to form a short-circuit current calculation model with positive and negative sequence decomposition, which accurately characterizes the transient characteristics of fault current under different voltage drops and effectively improves the accuracy of the calculation results.

1. Introduction

Since the proposal of the dual-carbon target, various types of clean energy generation methods have received widespread attention in the industry [1, 2]. Among them, the permanent magnet direct-drive wind power system has developed rapidly in recent years due to its outstanding advantages of abundant wind energy resources, stable wind speed, and so on [3]. In order to ensure that the phase angle and frequency of the voltage at the point of common coupling (PCC) can be detected quickly and accurately when the permanent magnet direct-drive wind power system is in the unbalanced operation state, the low-voltage ride-through control, including the positive and negative sequence decomposition link, is widely used in the permanent magnet direct-drive wind power system at present, so as to eliminate the disturbance caused by the negative sequence component to the system and realize the accurate phase lock based on the positive sequence component [4, 5]. Based on the above, the positive and negative sequence decomposition link has become an important part of the wind farm control strategy. At present, the most common methods of phase-locked loop based on positive sequence components are the dual second-order, generalised integrator phase-locked loop (DSOGI-PLL) [6], and the decoupled double synchronous reference frame phase-locked loop (DDSRF-PLL) [7]. Compared with DSOGI-PLL, the algorithm structure of DDSRF-PLL is more complex, and the decoupling structure of DDSRF-PLL is mainly aimed at eliminating the influence of the negative sequence fundamental frequency component, while the ability to resist low harmonic disturbance is relatively

weak [8, 9]. By contrast, the modelling process of frequency characteristics of the positive and negative sequence decomposition based on DSOGI-PLL is not only simple but can also eliminate the disturbance of the negative sequence fundamental voltage. Therefore, DSOGI-PLL is more widely used in practical applications [10].

When a fault occurs in the permanent magnet direct-drive wind power system, which leads to a three-phase symmetric drop of the voltage at the PCC point, it is of great significance to accurately analyze the transient characteristics of the fault current for the research of relay protection and fault treatment. The analysis methods of fault current are usually divided into steady-state analysis and transient analysis. Steady-state fault current analysis generally considers the role of low-voltage ride-through control and calculates steady-state current through sequence network analysis, and many research studies have been carried out in the industry [11]. Most literature equivalents the wind farm in steady state after a short-circuit fault to a controlled voltage source or a controlled current source and establishes a composite network under different fault conditions to simplify the modelling program of fault analysis and calculation [12].

The analysis of transient short-circuit current considers the influence of converter control, PLL, and other links and calculates the transient current value by writing down control equations and equivalent circuit differential equations. Compared with steady-state current calculation, transient current calculation is more complex. The industry has also carried out extensive research and achieved some results in consideration of its important role in studying the action behavior of relay protection. On the basis of the comprehensive analysis of the converter power supply control system, a calculation model of the fault current of the converter power supply with a low-voltage ride-through control strategy is proposed in [13], and the transient short-circuit current of the converter power supply is calculated by using the transfer functions in the complex frequency domain of both the control system and converter [14], starting with the mathematical model of the control system, which describes the output current of the inverter after the fault in the form of second-order, constant coefficient differential equations, and the current expression in the transient process is obtained analytically based on the steady-state value before and after the fault and the transient change law affected by the control parameters. The authors of [15] describe the positive and negative sequence current after fault as second-order, constant coefficient differential equations, and the short-circuit current expressions based on the independent control strategy of positive and negative sequence are derived. At last, it is concluded in [15] that the transient current is independent of the parameters of the outer power loop and is only affected by the control parameters of the inner current loop. Both [14, 15] regard the equation of the control system and the circuit equation as constant coefficient equations, which do not consider the influence of the nonlinear links in the control system on the transient characteristics of fault current. In view of the influence of nonlinear links in the control system on the transient current, the study [16] describes the output current as a second-order differential equation set with variable coefficients when there is an error between PLL output angular frequency and frequency compensation angular frequency and proposes a mathematical method based on the form of decoupling complex domain to solve the transient current of dq-axis [17]. It puts forward the conclusion that the dynamic process of PLL and its inductance connected to the power grid makes the control system of the grid-side converter of the wind farm produce positive feedback and amplify the oscillation of subsynchronous frequency. By considering the saturation characteristics of the current inner loop, the nonlinear differential equations of symmetric transient fault current are deduced, and an analysis method based on the phase plane is proposed to obtain the analytical expression of transient current in [18, 19] uses linear control theory to solve the calculation problems caused by nonlinear links in the converter control system. By setting PI parameters, the second-order system is simplified into the first-order system, and then, the fault current of the dq-axis is calculated by the time-frequency domain transformation. The study [20] proposes a calculation method of instantaneous asymmetric fault current of converter, which analyzes compositions and characteristics of the fault current and then concludes that fault current is affected by a control loop, fault type, fault distance, and a nonlinear limiter. None of the above studies on transient fault current take into account the influence of positive and negative sequence decomposition in the low-voltage ride-through control strategy.

In view of the influence of positive and negative sequence decomposition on transient characteristics of fault current [21, 22], we propose a short-circuit analysis model of renewable energy converter under the control of positive and negative sequence decoupling based on DSOGI. The fault transient current is analyzed by using the model in the complex frequency domain, and the conclusion that the transient characteristics of fault current are related to the delay characteristics of positive and negative sequence decomposition is presented. In [21, 22], both of them take the positive and negative sequence decomposition link into account in the analysis process of fault current transient characteristics. However, they do not consider the influence of the voltage drop process and the possible transient response of the negative sequence current suppression strategy caused by the positive and negative sequence decomposition in the transient process.

In fact, the positive and negative sequence decomposition links increase the nonlinear links in the control system, resulting in more complex transient characteristics of the converter output transient current; therefore, the influence on not only the nonsymmetrical fault current transient characteristics but also the symmetrical fault current transient characteristics cannot be ignored. In view of such problems, the analysis method of the transient current fault characteristics considering the positive and negative sequence decomposition link is deeply studied in this paper, and mainly aiming at the situation of voltage symmetric drop at the PCC point caused by external faults of the permanent magnet direct-drive wind power system in order to accurately study the effect of positive and negative sequence decomposition on symmetric fault. This paper is organized as follows: Section 2

studies the transient characteristics of DSOGI, and reveals the reason why the transient properties should be considered. Section 3 studies the calculation results of fault current without considering the transient characteristics of DSOGI, and the problems existing in the existing research are illustrated. Based on the transient characteristics of positive and negative sequence decomposition described in Section 2, Section 4 establishes the time domain short circuit calculation model about fault current, and a fault current transient analysis method is proposed based on this model. In view of different voltage drops, in Section 5, the calculation results of transient current under different voltage drops are obtained by using the calculation model, and the transient characteristics of fault current when considering the transient characteristics of DSOGI are illustrated. Section 6 draws the conclusions.

2. Control Strategy of a Grid-Side Converter of Permanent Magnet Direct-Drive Wind Turbine with Positive-Negative Sequence Decomposition

The grid-connected delivery system of the permanent magnet direct-drive wind power system is shown in Figure 1. The stator windings of the permanent magnet wind generator are collected by the converter and then connected to the transmission network by the transformer [23].

When the three-phase fault of the remote AC system leads to voltage drop at the point of common coupling (PCC), if the voltage drop is deep enough to cause the power imbalance between the two ends of the DC side of the converter, the chopper circuit on the DC side will be input to keep the DC voltage stable. Therefore, the machine-side converter has little influence on the transient current output of the AC system. At this time, the transient process of the fault current output from the wind farm mainly depends on the response characteristics of the control system of the grid-side converter (GSC) during the fault. Thus, this paper mainly analyzes the influence of the GSC control strategy on the transient characteristics of fault current.

2.1. The Positive and Negative Sequence Decomposition of a Grid-Side Converter. In order to ensure that the PLL can accurately lock the phase of the fundamental positive sequence component when the power grid is in a three-phase unbalanced state, the voltage at the PCC point u_{abc} will be decomposed into positive and negative sequence at first. The basic structure of the DSOGI-PLL which is commonly used is shown in Figure 2 [24, 25].

In the structure of Figure 2, "**C**" is the Clark transformation matrix, and the "P" is the Parker transformation matrix.

It can be learned from Figure 2 that the voltages at the PCC point u_a, u_b, and u_c are translated from the abc three-phase coordinate frame to the $\alpha\beta$two-phase stationary coordinate frame to obtain u'_α and u'_β:

$$\begin{pmatrix} u'_\alpha \\ u'_\beta \end{pmatrix} = C \cdot \begin{pmatrix} u_a \\ u_b \\ u_c \end{pmatrix}. \tag{1}$$

By using the second-order generalized integrator which has the characteristic of frequency selection and can extract the fundamental voltage component of the input signal u'_α, the output signal qu'_α which has the same amplitude with u'_α but the phase lags u'_α 90°, and the output signal u_a which has the same amplitude and phase with u'_α can be obtained. Their relationships can be expressed as

$$\begin{aligned} G_1(s) &= \frac{u_\alpha(s)}{u'_\alpha(s)} = \frac{k\omega_{\mathrm{PLL}}s}{s^2 + k\omega_{\mathrm{PLL}}s + {\omega_{\mathrm{PLL}}}^2}, \\ G_2(s) &= \frac{qu_\alpha(s)}{u'_\alpha(s)} = \frac{k{\omega_{\mathrm{PLL}}}^2}{s^2 + k\omega_{\mathrm{PLL}}s + {\omega_{\mathrm{PLL}}}^2}, \end{aligned} \tag{2}$$

where k is the damping factor. In order to give consideration to filtering effect and response speed, the value of k is usually 2. q is a phase shift operator with a lag of 90 degrees. qu'_β and u'_β can also be obtained by equation (2).

The positive sequence voltages in the two-phase stationary coordinate frame u^+_α and u^+_β can be obtained by the following equation:

$$\begin{aligned} u^+_\alpha &= \frac{1}{2}\left(u_\alpha - qu_\beta\right), \\ u^+_\beta &= \frac{1}{2}\left(qu_\alpha + u_\beta\right). \end{aligned} \tag{3}$$

The parker transformation is used to transform u^+_α and u^+_β to the dq-axis coordinate frame of positive sequence which rotates synchronously with the three-phase coordinate frame, and the dq-axis voltage components of positive sequence at the PCC point u^+_d and u^+_q are obtained. The process of the Parker transformation can be expressed as

$$\begin{pmatrix} u^+_d \\ u^+_q \end{pmatrix} = P \cdot \begin{pmatrix} u^+_\alpha \\ u^+_\beta \end{pmatrix}. \tag{4}$$

The produce process of θ_{PLL} is as follows: the PLL regulates u^+_q to zero by using the PI controller and error adjustment which can obtain the angular frequency ω_{PLL}, and then feedback the value to DSOGI. After ω_{PLL} is integrated, the phase angle θ_{PLL} can be obtained and fed back into the Parker transformation matrix:

$$\begin{cases} \omega_{\mathrm{PLL}} = k_{\mathrm{pPLL}}\left(-u^+_q\right) + k_{\mathrm{iPLL}}\int\left(-u^+_q\right)\mathrm{d}t + \omega_0, \\ \theta_{\mathrm{PLL}} = \omega_{\mathrm{PLL}}t. \end{cases} \tag{5}$$

In equation (7), k_{pPLL} and k_{iPLL} represent the proportional and integral coefficients of the phase-locked loop PI controller, respectively. The value of ω_0 is typically set to 100π rad/s.

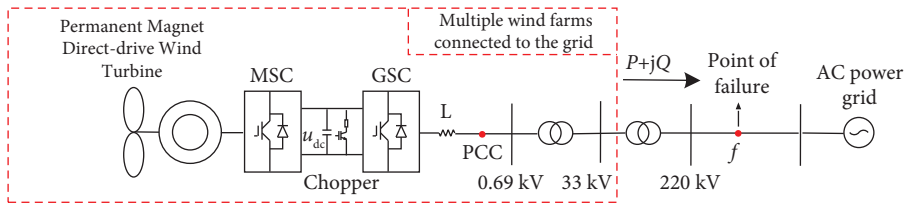

Figure 1: Schematic diagram of a permanent magnet direct-drive wind power system.

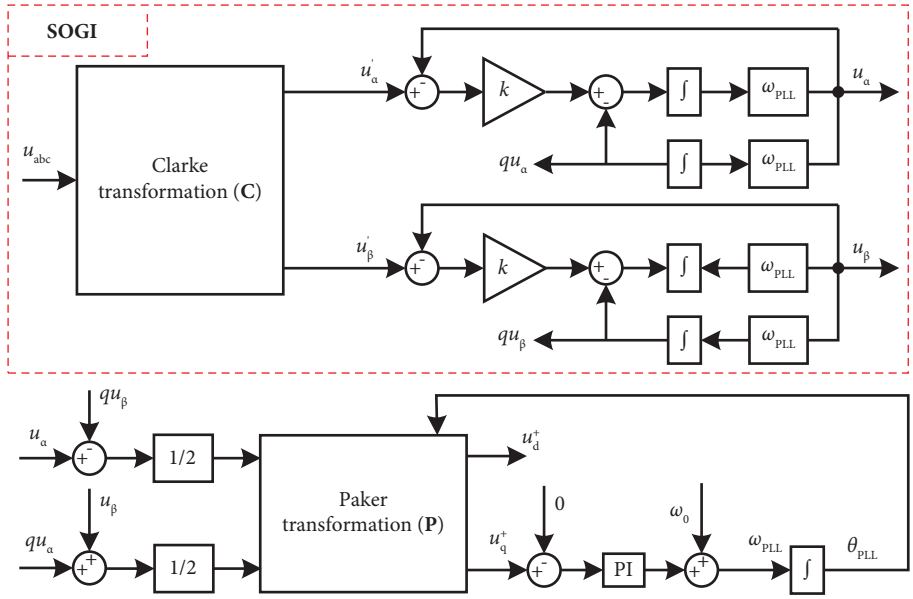

Figure 2: The structure of DSOGI-PLL.

2.2. Low-Voltage Ride-Through Control Strategy of a Permanent Magnet Direct-Drive Wind Power System. According to the standard of the low-voltage ride-through capability of a grid-connected wind farm, the permanent magnet direct-drive wind power system should not only keep connected to the power grid during the low-voltage ride-through but also provide reactive current to support the grid voltage [26, 27]. The control strategy of GSC after failure is shown in Figure 3.

The basic principle of the low-voltage ride-through control strategy is when u_{abc} drops, the control system should detect the drop magnitude of positive sequence voltage at the PCC point u_{PCC} and determine the reference value of active current i_d^* and reactive current i_q^* according to the drop magnitude of u_{PCC}. When the magnitude of u_{PCC} does not drop to 90%, the control strategy remains unchanged; it means that the dq-axis current reference values of current inner loop control i_d^* and i_q^* are generated by the voltage outer loop control which are the same as the normal control strategy. When the magnitude of u_{PCC} drops to 90%, the GSC is required to provide a certain reactive power support. In order to improve the speed of reactive response, i_q^* is generated without the outer loop control, but the outer loop control of reactive power is switched to the direct current inner loop control, and i_d^* is decided by i_q^*. The final control target is the output fault current of GSC i_{abc} after external fault does not exceed 1.2 times the rated current according to the tolerance ability of short-circuit current of converter [28, 29].

Based on the low-voltage ride-through control strategy, i_d^* and i_q^* can be regarded as functions about u_{PCC}; thus, their relationships can be expressed as

$$\begin{cases} i_d^* = i_{d-pi}^* \cdot \varepsilon\left(u_{PCC} - u'_{PCC}\right) + \varepsilon\left(u_{PCC} - 0.1\right) \cdot \sqrt{1.2^2 - \left(1.5 \times \left(0.9 - u_{PCC}\right)^2\right)} \\ - \varepsilon\left(u_{PCC} - u'_{PCC}\right) \cdot \sqrt{1.2^2 - \left(1.5 \times \left(0.9 - u_{PCC}\right)^2\right)}, \\ i_q^* = \varepsilon\left(u_{PCC} - 0.1\right) \cdot 1.5 \times \left(0.9 - u_{PCC}\right) - \varepsilon\left(u_{PCC} - 0.9\right) \cdot 1.5 \times \left(0.9 - u_{PCC}\right) \\ + 1.2 - \varepsilon\left(u_{PCC} - 0.1\right) \times 1.2, \end{cases} \tag{6}$$

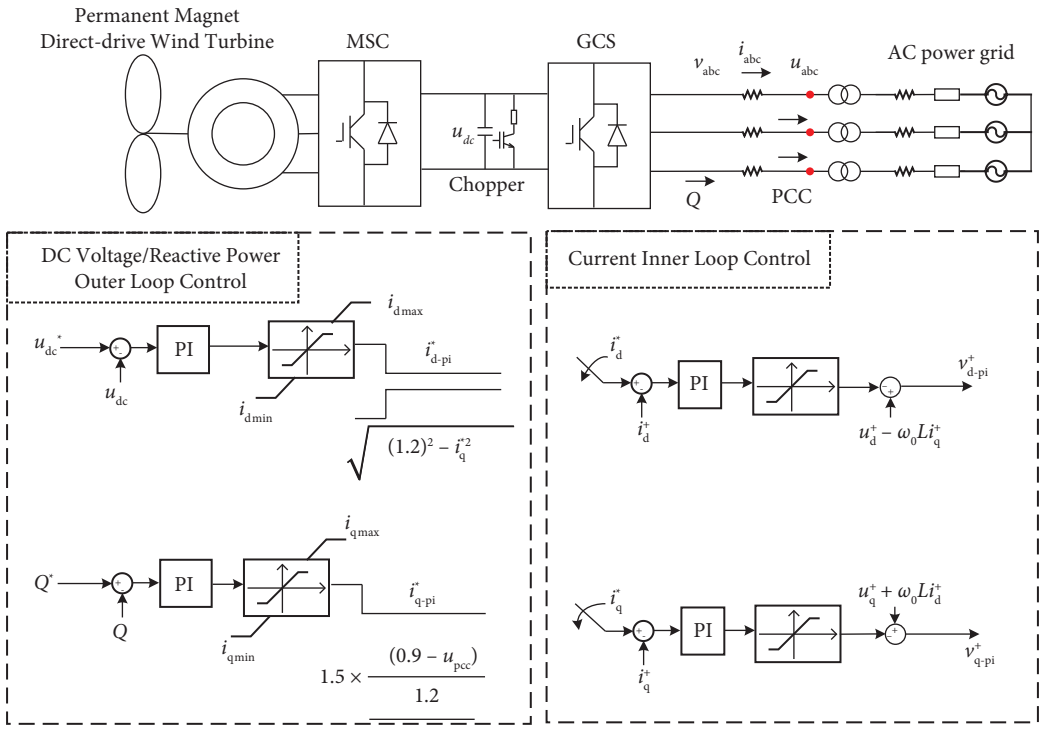

Figure 3: Control strategy of a grid side converter.

where $\varepsilon(u_{\mathrm{PCC}})$ is the step function; and $i^*_{d-\mathrm{pi}}$ and $i^*_{q-\mathrm{pi}}$ are the current inner loop reference values generated by the voltage outer loop, and can be expressed as

$$\begin{cases} i^*_{d-\mathrm{pi}} = k_{\mathrm{up}}\left(u^*_{\mathrm{dc}} - u_{\mathrm{dc}}\right) + k_{\mathrm{ui}}\int\left(u^*_{\mathrm{dc}} - u_{\mathrm{dc}}\right)\mathrm{d}t, \\ i^*_{q-\mathrm{pi}} = k_{\mathrm{up}}\left(Q^* - Q\right) + k_{\mathrm{ui}}\int\left(Q^* - Q\right)\mathrm{d}t. \end{cases} \tag{7}$$

u'_{PCC} represents the PCC point voltage when the d-axis control strategy switches to direct current control and can be expressed as

$$u'_{\mathrm{PCC}} = 0.9 - \frac{\sqrt{(1.2)^2 - \left(i^*_{d-\mathrm{pi}}\right)^2}}{1.5}. \tag{8}$$

According to (5), taking the system working in rated state during normal operation as an example, the change process of i^*_d and i^*_q is shown in Figure 4 when the magnitude of u_{PCC} drops by more than 10% after failure.

It can be learned from Figure 4. That before the failure i^*_d is 1 p.u. and i^*_q is 0 p.u. when the system is running in the rated state. When the magnitude of u_{PCC} is more than 90%, i^*_d and i^*_q will still be determined by the outer loop control; when the magnitude of u_{PCC} is less than 90%, the control of q-axis will switch to current inner loop control. At this point, i^*_q changes with the magnitude of u_{PCC}, while i^*_d is still generated by outer loop control. When the magnitude of u_{PCC} is less than u'_{PCC}, the control of d-axis will be switched to direct current control, and i^*_d is calculated according to the root (1.2^2-i^{*2}_q). When the magnitude of u_{PCC} is less than 10%, i^*_q reaches the limiting value of 1.2 p.u., and i^*_d is 0 p.u.

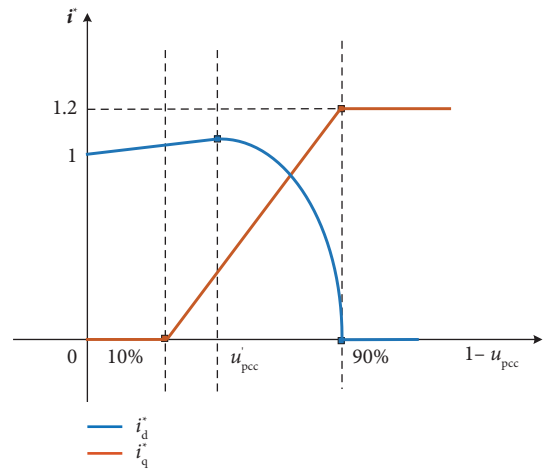

Figure 4: The reference value of dq-axis current.

3. Transient Current Calculation Based on Existing Research Methods

The existing method of calculating the GSC output currents i_a, i_b, and i_c do not consider the positive and negative sequence decomposition. In the process of solving, the circuit equation between the voltages at the PCC point u_a, u_b, and u_c and the output voltages of GSC v_a, v_b, and v_c are transformed to the dq-axis coordinate frame of positive sequence, and then the equation is solved simultaneously with the equation of inner loop control [12]. The circuit equation in abc three-phase coordinate frame can be expressed as

$$\begin{pmatrix} v_a \\ v_b \\ v_c \end{pmatrix} = L\frac{d}{dt}\begin{pmatrix} i_a \\ i_b \\ i_c \end{pmatrix} + \begin{pmatrix} u_a \\ u_b \\ u_c \end{pmatrix}. \tag{9}$$

In equation (9), L is the equivalent inductance of the filter between v_a, v_b, and v_c and u_a, u_b, and u_c. When the circuit equation in three-phase coordinate frame is transformed to the dq-axis coordinate frame of positive sequence, the influence of positive and negative sequence decomposition link on the process of coordinate transformation is not taken into account in the existing research method since the research object is the three-phase symmetrical fault. Therefore, the circuit equation in the dq-axis coordinate frame of the positive sequence is obtained by multiplying both sides of equation (9) by the Parker transformation matrix P directly, which can be expressed as

$$\begin{cases} v_d^+ = L\dfrac{d}{\mathrm{d}t}i_d^+ - \omega_{\mathrm{PLL}}Li_q^+ + u_d^+, \\ \\ v_q^+ = L\dfrac{d}{\mathrm{d}t}i_q^+ + \omega_{\mathrm{PLL}}Li_d^+ + u_q^+, \end{cases} \tag{10}$$

where i_d^+ and i_q^+ are the dq-axis output currents of positive sequence by GSC; and v_d^+ and v_q^+ are the dq-axis output voltages of positive sequence by GSC.

The equation of current inner loop control can be expressed as [22]

$$\begin{cases} v_{d-\mathrm{pi}}^+ = \left[k_{\mathrm{ip}}\left(i_d^* - i_d^+\right) + k_{\mathrm{ii}}\int\left(i_d^* - i_d^+\right)\mathrm{d}t\right] - \omega_0\mathrm{L}i_q^+ + u_d^+, \\ v_{q-\mathrm{pi}}^+ = \left[k_{\mathrm{ip}}\left(i_q^* - i_q^+\right) + k_{\mathrm{ii}}\int\left(i_q^* - i_q^+\right)\mathrm{d}t\right] + \omega_0\mathrm{L}i_d^+ + u_q^+, \end{cases} \tag{11}$$

where $v_{d-\mathrm{pi}}^+$ and $v_{q-\mathrm{pi}}^+$ are the output voltage modulation signals of GSC generated by the inner loop of the control system. k_{ip} is the proportional gain and k_{ii} is the integral time constant of the inner loop PI controller.

The existing method suggest that $v_d^+ = v_{d-\mathrm{pi}}^+$ and $v_q^+ = v_{q-\mathrm{pi}}^+$. By combining equation (10) with equation (11), taking v_d^+ and v_q^+ as intermediate variables and eliminating them, the differential equations of i_d^+ and i_q^+ can be obtained:

$$\begin{cases} 0 = -L\dfrac{d}{\mathrm{d}t}i_d^+ + \omega_{\mathrm{PLL}}\mathrm{L}i_q^+ + \left[k_{\mathrm{ip}}\left(i_d^* - i_d^+\right) + k_{\mathrm{ii}}\int\left(i_d^* - i_d^+\right)\mathrm{d}t\right] - \omega_0\mathrm{L}i_q^+, \\ 0 = -L\dfrac{d}{\mathrm{d}t}i_q^+ - \omega_{\mathrm{PLL}}\mathrm{L}i_d^+ + \left[k_{\mathrm{ip}}\left(i_q^* - i_q^+\right) + k_{\mathrm{ii}}\int\left(i_q^* - i_q^+\right)\mathrm{d}t\right] + \omega_0\mathrm{L}i_d^+, \end{cases} \tag{12}$$

where i_d^+ and i_q^+ can be obtained by solving (9) with the Runge–Kutta method. The object of study is a three-phase short-circuit fault. Therefore, the transient component of negative sequence is very small and is generally not considered. i_{a}, i_{b}, and i_{c} can be obtained by directly performing the Parker inverse transformation on the dq-axis current of positive sequence.

It is assumed that the magnitude of u_{PCC} drop to 7% of the rated voltage when an external fault occurs, and the calculation results of equation (12) are compared with the simulation results of the control system containing positive and negative sequence decomposition link. The results are shown in Figures 5(a) and 5(b).

It can be seen from Figures 5(a) and 5(b) that due to the absence of the influence of positive and negative sequence decomposition link, i_d^+ and i_q^+ obtained by the existing research method have a large error in comparison with the simulation result, and the overshoot and oscillation attenuation characteristics of their transient process cannot be reflected. Therefore, the existing research method is no longer suitable for studying the transient characteristics of fault current with positive and negative sequence decomposition.

According to the analysis in Section 3, in order to accurately analyze the transient characteristics of the fault current containing the positive and negative sequence decomposition link, the transient process of the positive and negative sequence decomposition link should also be taken into account.

4. Study on Transient Process of Positive and Negative Sequence Decomposition

4.1. Analysis of the Transient Response of DSOGI-PLL. The transient response process of DSOGI-PLL is studied by taking the symmetrical fault of the AC system as an example. It is supposed that a three-phase fault occur in the AC system at 2 s, and at this time, the magnitude of u_{PCC} will drop to 7% of the rated voltage. When there is a symmetrical fault in the line, the voltage at the fault point can be regarded as the voltage will change to 0 in a very short time. Due to the short line of the permanent magnet direct drive wind power system, the voltage at the PCC point can also be regarded as the instantaneous sudden change voltage, thus simplifying the calculation of subsequent fault current. The waveform of the voltage at the PCC point in the two-phase stationary coordinate frame $u'_\alpha$is shown by the blue curve in Figure 5. It can be considered that the change of u'_α caused by external fault is basically seen as an instantaneous drop, and the specific expression can be expressed as

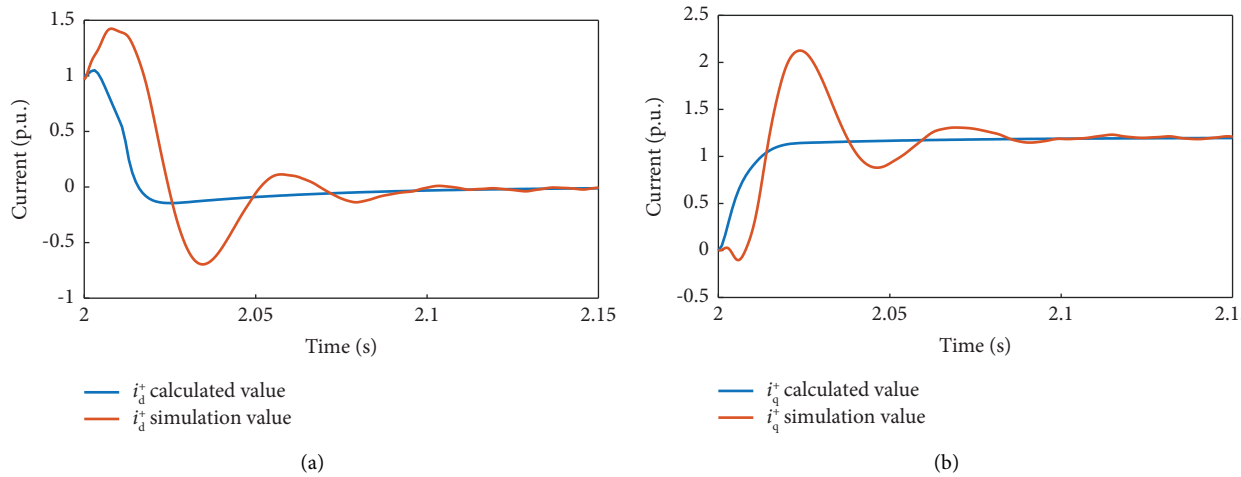

Figure 5: GSC's output current of the positive sequence under external three-phase fault. (a) d-axis output current of positive sequence and (b) q-axis output current of positive sequence.

$$u'_\alpha = U\cos(\omega_0 t) + [0.07U\sin(\omega_{\mathrm{PLL}} t) - U\cos(\omega_0 t)] \cdot \varepsilon(t - t_0). \tag{13}$$

After the SOGI link, the output waveforms of u_α and qu_α are shown by the red and yellow curves in Figure 6, respectively.

It can be learned from Figure 6 that the transient process of the output signal u_α of the SOGI link after failure is not exactly the same as the input signal u_α. The amplitude and phase of u_α cannot track the changes in the amplitude and phase of u'_α. Under the simulation parameters in this paper, about 20 ms of transient process are needed to achieve steady-state tracking. qu_α also tends to be stable after a transient process of about 20 ms.

u_α, qu_α, u_β, and qu_β generated by the SOGI link are used to calculate the dq-axis voltage components of positive sequence at the PCC point u_d^+ and u_q^+ by (4), and the comparison results of u_d^+, u_q^+ and the voltages of dq-axis u_d, u_q that do not include the positive and negative sequence decomposition link are shown in Figures 7(a) and 7(b).

It can be learned from Figures 7(a) and 7(b) that after the positive and negative sequence decomposition, both u_d^+ and u_q^+ have transient processes for a certain period of time, and the amplitudes change greatly. However, u_d and u_q obtained without positive and negative sequence decomposition have small amplitude changes and short durations in the transient processes.

It can be learned from the analysis of the transient characteristics of DSOGI-PLL that when the voltage at the PCC point drops, the output signal of the SOGI link will go through a transient process to track the amplitude and phase of the changed actual three-phase voltage, although the actual three-phase voltage at the PCC point can be approximately regarded as instantaneous drop. As a result, u_d^+ and u_q^+ also need to go through a transient process to reach the steady state. It can be learned from equation (4) that u_d^+ and u_q^+ will affect the drop process of the positive sequence voltage u_{PCC} at the PCC point and then affect the change processes of current reference values of dq-axis i_d^* and i_q^* through equation (6).

According to the analysis in Section 4.1, the transient fluctuation processes of u_d^+ and u_q^+ calculated after the positive and negative sequence decomposition is obvious. Therefore, the influence of this decomposition process should be taken into account in the transient analysis of symmetrical fault current.

4.2. Circuit Equation in dq-Axis Coordinate Frame of Positive Sequence including the Positive and Negative Sequence Decomposition. Since the control of the GSC is based on the dq-axis coordinate frame of positive sequence, in order to study the transient characteristics of the output fault currents i_a, i_b, and i_c of GSC, it is necessary to transform the circuit equation between the voltages u_a, u_b, and u_c at the PCC point and the output voltages of GSC v_a, v_b, and v_c from the three-phase coordinate frame to the dq-axis coordinate frame of positive sequence. Due to space limitations, this paper analyzes and calculates the positive sequence current under symmetric faults and verifies the accuracy of the calculation model. According to the analysis in Section 2.1, the transformation process of the circuit equation is changed after the positive and negative sequence decomposition is added to the control strategy. Therefore, the coordinate transformation process of the voltage equation should be analyzed in detail.

The equation in the $\alpha\beta$ two-phase stationary coordinate frame can be obtained from equation (6) by the Clarke transformation:

$$\begin{pmatrix} v'_\alpha \\ v'_\beta \end{pmatrix} = L\frac{d}{dt}\begin{pmatrix} i'_\alpha \\ i'_\beta \end{pmatrix} + \begin{pmatrix} u'_\alpha \\ u'_\beta \end{pmatrix}, \tag{14}$$

where v'_α and v'_β are the output voltages of GSC in the two-phase stationary coordinate frame; i'_α and i'_β are the output currents of GSC in the two-phase stationary coordinate

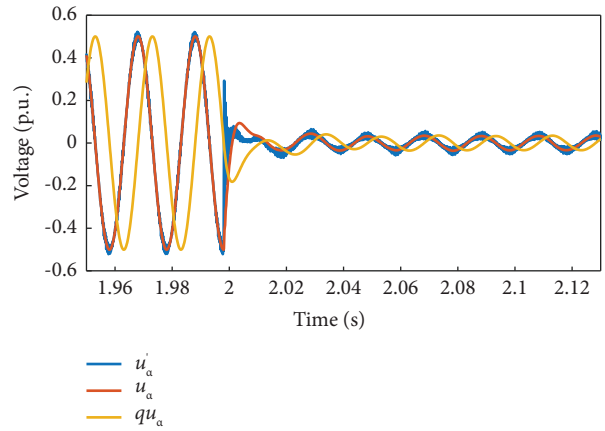

Figure 6: Input signal and output signal of SOGI link.

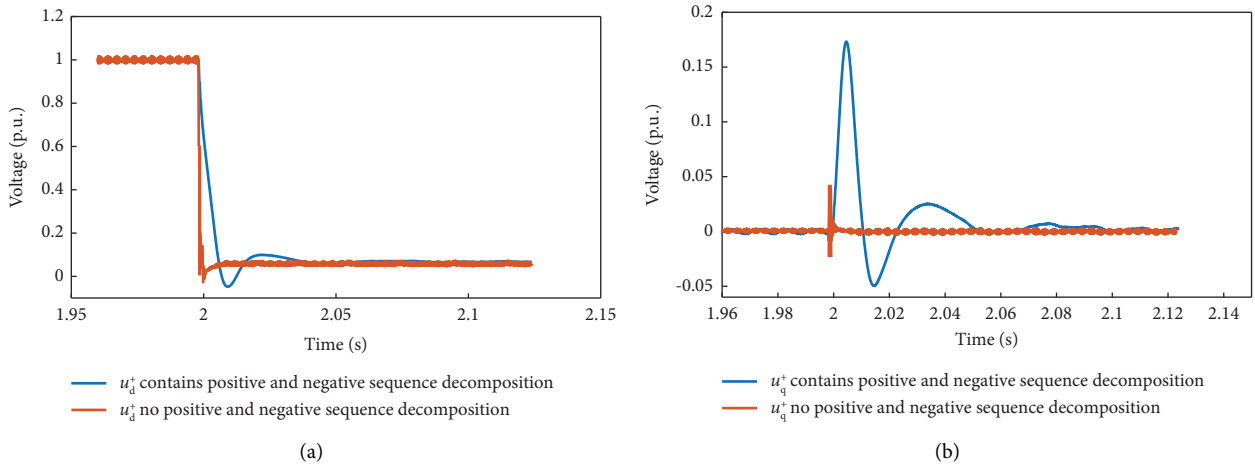

Figure 7: The voltages at the PCC point of dq-axis. (a) d-axis voltage and (b) q-axis voltage.

frame. According to the analysis in Section 2.1, the SOGI link can use the transfer functions in the complex frequency domain to represent the relationship between the input signal and the output signal. Therefore, before the positive and negative sequence decomposition, the Laplace transform of equation (14) is first carried out to obtain the circuit equation in the complex frequency domain of the two-phase stationary coordinate frame:

$$\begin{pmatrix} v'_\alpha(s) \\ v'_\beta(s) \end{pmatrix} = \begin{pmatrix} si'_\alpha(s) - i'_\alpha(t_0) \\ si'_\beta(s) - i'_\beta(t_0) \end{pmatrix} + \begin{pmatrix} u'_\alpha(s) \\ u'_\beta(s) \end{pmatrix}, \tag{15}$$

where $i'_\alpha(t_0)$ and $i'_\beta(t_0)$ are the initial values of the output currents of GSC in the two-phase stationary coordinate frame when the fault occurs.

The coordinate transformation method adopted by the SOGI link is applied to equation (15), and the GSC output voltages $v^+_\alpha(s)$ and $v^+_\beta(s)$ of positive sequence in the two-phase stationary coordinate frame are

$$\begin{aligned} \begin{pmatrix} v^+_\alpha(s) \\ v^+_\beta(s) \end{pmatrix} &= L\begin{pmatrix} \frac{1}{2}G_1(s) & -\frac{1}{2}G_2(s) \\ \frac{1}{2}G_2(s) & \frac{1}{2}G_1(s) \end{pmatrix}\begin{pmatrix} si'_\alpha(s) - i'_\alpha(t_0) \\ si'_\beta(s) - i'_\beta(t_0) \end{pmatrix} \\ &+ \begin{pmatrix} \frac{1}{2}G_1(s) & -\frac{1}{2}G_2(s) \\ \frac{1}{2}G_2(s) & \frac{1}{2}G_1(s) \end{pmatrix}\begin{pmatrix} u'_\alpha(s) \\ u'_\beta(s) \end{pmatrix}. \end{aligned} \tag{16}$$

The transfer functions $G_1(s)$ and $G_2(s)$ in equation (2) are substituted into (13) and simplified to obtain

$$\begin{pmatrix} v^+_\alpha(s) \\ v^+_\beta(s) \end{pmatrix} = L\begin{pmatrix} si^+_\alpha(s) - i^+_\alpha(t_0) \\ si^+_\beta(s) - i^+_\beta(t_0) \end{pmatrix} + \begin{pmatrix} u^+_\alpha(s) \\ u^+_\beta(s) \end{pmatrix} + L\begin{pmatrix} f_1(s) \\ f_2(s) \end{pmatrix}, \tag{17}$$

where $i_\alpha^+(t_0)$ and $i_\beta^+(t_0)$ are the initial values of positive sequence currents output by GSC in the two-phase stationary coordinate frame at the fault moment; and $f_1(s)$ and $f_2(s)$ are the oscillation attenuation components generated in the simplification process, and the specific expressions can be expressed as

$$\begin{cases} f_1(s) = i_\alpha^+(t_0) - \dfrac{1}{2}G_1(s)i_\alpha'(t_0) + \dfrac{1}{2}G_2(s)i_\beta'(t_0), \\ f_2(s) = i_\beta^+(t_0) - \dfrac{1}{2}G_2(s)i_\alpha'(t_0) - \dfrac{1}{2}G_1(s)i_\beta'(t_0). \end{cases} \tag{18}$$

Transform (14) into the time domain:

$$\begin{pmatrix} v_\alpha^+ \\ v_\beta^+ \end{pmatrix} = L\frac{d}{dt}\begin{pmatrix} i_\alpha^+ \\ i_\beta^+ \end{pmatrix} + \begin{pmatrix} u_\alpha^+ \\ u_\beta^+ \end{pmatrix} + L\begin{pmatrix} f_1(t) \\ f_2(t) \end{pmatrix}, \tag{19}$$

where i_α^+ and i_β^+ are the GSC output currents of positive sequence in the two-phase stationary coordinate frame.

Parker transformation is applied to equation (19) to obtain the circuit equations in the dq-axis coordinate frame of positive sequence:

$$\begin{cases} v_d^+ = L\dfrac{d}{dt}i_d^+ - \omega_{PLL}Li_q^+ + u_d^+ + L\left(\cos\theta_{PLL}f_1(t) + \sin\theta_{PLL}f_2(t)\right), \\ v_q^+ = L\dfrac{d}{dt}i_q^+ + \omega_{PLL}Li_d^+ + u_q^+ + L\left(-\sin\theta_{PLL}f_1(t) + \cos\theta_{PLL}f_2(t)\right), \end{cases} \tag{20}$$

where v_d^+ and v_q^+ are the calculated output voltages of GSC in the dq-axis coordinate frame of positive sequence by the DSOGI-PLL link. In the low-voltage ride-through control strategy, the output voltage modulation signals of GSC generated by the inner loop of the control system in the dq-axis coordinate frame of positive sequence v_{d-pi}^+ and v_{q-pi}^+ are determined by the output results of the current inner loop of the positive sequence. If the transient response of the positive and negative sequence decomposition leads to $v_d^+ \neq v_{d-pi}^+$ and $v_q^+ \neq v_{q-pi}^+$, v_d^+ and v_q^+ will not be used as intermediate variables to eliminate and simplify the equations when the circuit equation of the dq-axis coordinate frame of the positive sequence and the equation of the low-voltage ride-through control strategy are combined. Therefore, the following mainly focuses on the relationships between v_d^+ and v_{d-pi}^+ as well as v_q^+ and v_{q-pi}^+.

4.3. Analysis of Transient Characteristics of GSC Output Current in the dq-Axis of Positive Sequence. The inner loop of the control system is often designed with the steady-state circuit equation of the main loop. When the positive and negative sequence decomposition link is added to the control system, the dq-axis output currents of positive sequence by GSC i_d^+, i_q^+, and the dq-axis voltages of positive sequence at the PCC point u_d^+ and u_q^+ are used for the current inner loop control to calculate the output voltage modulation signals v_{d-pi}^+ and v_{q-pi}^+ of GSC in the dq-axis coordinate frame of positive sequence. The response equations of current inner loop control can be expressed as

$$\begin{cases} v_{d-pi}^+ = \left[k_{ip}\left(i_d^* - i_d^+\right) + k_{ii}\int\left(i_d^* - i_d^+\right)dt\right] - \omega_0 Li_q^+ + u_d^+, \\ v_{q-pi}^+ = \left[k_{ip}\left(i_q^* - i_q^+\right) + k_{ii}\int\left(i_q^* - i_q^+\right)dt\right] + \omega_0 Li_d^+ + u_q^+. \end{cases} \tag{21}$$

In the control system, the modulation method of output voltages of GSC v_a, v_b, and v_c is the dq-axis voltages of positive and negative sequence v_{d-pi}^+, v_{q-pi}^+, v_{d-pi}^-, and v_{q-pi}^- obtained from the current inner loop of the positive and negative sequence are transformed to abc three-phase coordinate frame by parker inverse transformation, and then superimpose them to generate the three-phase modulation wave, whose values are equal to the output voltages of GSC v_a, v_b, and v_c. Therefore, the relationship can be expressed as

$$\begin{pmatrix} v_a \\ v_b \\ v_c \end{pmatrix} = C^{-1}\cdot P_{\theta_{PLL}}^{-1}\begin{pmatrix} v_{d-pi}^+ \\ v_{q-pi}^+ \end{pmatrix} + C^{-1}\cdot P_{-\theta_{PLL}}^{-1}\begin{pmatrix} v_{d-pi}^- \\ v_{q-pi}^- \end{pmatrix}, \tag{22}$$

where "$P_{\theta PLL}{}^{-1}$" is the Parker inverse transformation matrix of positive components, and "$P_{-\theta PLL}{}^{-1}$" is the Parker inverse transformation matrix of negative components.

According to the coordinate transformation process described in Section 4.2, coordinate transformation, including positive and negative sequence decomposition link, is performed on equation (22). After the positive and negative sequence decomposition link is applied to equation (22), the decoupling of positive and negative sequence equation can be obtained. With the positive order equation being taken into consideration only, the relations of v_d^+, v_q^+, v_{d-pi}^+, and v_{q-pi}^+ can be expressed as

$$\begin{aligned} v_d^+ = {} & \cos\theta_{PLL}\cdot g_1(t) * \left(\cos\theta_{PLL}\cdot v_{d-pi}^+ - \sin\theta_{PLL}\cdot v_{q-pi}^+\right) \\ & + \sin\theta_{PLL}\cdot g_1(t) * \left(\sin\theta_{PLL}\cdot v_{d-pi}^+ + \cos\theta_{PLL}\cdot v_{q-pi}^+\right), \end{aligned} \tag{23}$$

$$\begin{aligned} v_q^+ = {} & \cos\theta_{PLL}\cdot g_1(t) * \left(\sin\theta_{PLL}\cdot v_{d-pi}^+ + \cos\theta_{PLL}\cdot v_{q-pi}^+\right) \\ & - \sin\theta_{PLL}\cdot g_1(t) * \left(\cos\theta_{PLL}\cdot v_{d-pi}^+ - \sin\theta_{PLL}\cdot v_{q-pi}^+\right), \end{aligned} \tag{24}$$

where " $*$ " stands for convolution, "$\cdot$" stands for the product, and $g_1(t)$ and $g_2(t)$ are the expressions of SOGI transfer functions $G_1(s)$ and $G_2(s)$ reduced to the time domain, respectively.

According to equations (23) and (24), by the coordinate transformation, including the positive and negative sequence decomposition, the circuit equation on the left side of the equal sign can obtain the positive sequence components v_d^+ and v_q^+, which are the same as those in equation (20), and the specific relationships between v_d^+ and v_q^+ and $v_{d-\mathrm{pi}}^+$ and $v_{q-\mathrm{pi}}^+$ are obtained. It can also be learned from equations (23) and (24) that $v_d^+ \neq v_{d-\mathrm{pi}}^+$ and $v_q^+ \neq v_{q-\mathrm{pi}}^+$.

In order to verify the accuracy of the conclusion of $v_d^+ \neq v_{d-\mathrm{pi}}^+$ and $v_q^+ \neq v_{q-\mathrm{pi}}^+$, the AC system is set to have a three-phase fault at 2s in the simulation, and the magnitude of positive sequence voltage at the PCC point u_{PCC} drops to about 7% when it reaches the steady state.

The parameters used in the simulation are shown in Table 1:

The simulation waveforms of v_d^+, v_q^+, $v_{d-\mathrm{pi}}^+$, and $v_{q-\mathrm{pi}}^+$ are obtained by PSCAD/EMTDC as shown in Figures 8(a) and 8(b).

It can be learned from Figures 8(a) and 8(b) that the dynamic processes of v_d^+ and $v_{d-\mathrm{pi}}^+$, v_q^+ and $v_{q-\mathrm{pi}}^+$ are significantly different, which verifies the correctness of the analysis results of $v_d^+ \neq v_{d-\mathrm{pi}}^+$ and $v_q^+ \neq v_{q-\mathrm{pi}}^+$ obtained from equations (23) and (24) in Section 4.3.

It can be learned that the positive and negative sequence decomposition link makes the circuit equation transformed to the dq-axis coordinate frame of positive sequence have great changes compared with the existing research method.

(1) The positive and negative sequence decomposition link makes the circuit equation have two more transient attenuation components $f_1(t)$ and $f_2(t)$ in the process of coordinate transformation.

(2) The positive and negative sequence decomposition link makes the output voltage modulation signals of GSC in the dq-axis coordinate frame of positive sequence $v_{d-\mathrm{pi}}^+$ and $v_{q-\mathrm{pi}}^+$ no longer equal to the calculated output voltage of GSC in the dq-axis coordinate frame of positive sequence v_d^+ and v_q^+ by the positive and negative sequence decomposition link.

Therefore, it is necessary to propose a research method that can take (1) and (2) into consideration in order to accurately analyze the transient characteristics of i_d^+ and i_q^+.

5. Study on Transient Characteristics of Fault Current including Positive and Negative Sequence Decomposition

5.1. The Solution Method of dq-Axis Output Current of Positive Sequence by GSC. According to the analysis in Section 4, there are differences between v_d^+ and $v_{d-\mathrm{pi}}^+$ and v_q^+ and $v_{q-\mathrm{pi}}^+$ due to the transient responses of positive and negative sequence decomposition link. Although (20) and (21) can represent their relations, it is difficult to obtain the specific differences of their transient processes according to the equation. Therefore, in order to find out whether there is a transient process expression with obvious law between v_d^+ and $v_{d-\mathrm{pi}}^+$ and v_q^+ and $v_{q-\mathrm{pi}}^+$, the waveforms of $v_d^+ - v_{d-\mathrm{pi}}^+$ and $v_q^+ - v_{q-\mathrm{pi}}^+$ should be observed first, which are shown in Figure 9.

According to Figure 9, when the magnitude of positive sequence voltage at the PCC point u_{PCC} drops to about 7%, $v_d^+ - v_{d-\mathrm{pi}}^+$ and $v_q^+ - v_{q-\mathrm{pi}}^+$ can be approximately regarded as attenuating and oscillating waveforms, and they tend to be stable after a transient process which means the differences of both $v_d^+ - v_{d-\mathrm{pi}}^+$ and $v_q^+ - v_{q-\mathrm{pi}}^+$ are 0. These transient processes fluctuate greatly and last for a long time, the durations are about 80 ms.

According to the characteristics of waveform shown in Figure 9, MATLAB is used to fit the oscillation attenuation waveforms $v_d^+ - v_{d-\mathrm{pi}}^+$ and $v_q^+ - v_{q-\mathrm{pi}}^+$ with the third-order and the fourth-order oscillation attenuation function, respectively, when the magnitude of u_{PCC} drops to about 7%, which can be expressed as

$$\begin{aligned} v_d^+ - v_{d-\mathrm{pi}}^+ = {} & 3.104 \times e^{-152.9t} \times \sin(2\pi \times 40 \times t) \\ & - 0.6628 \times e^{-116.1t} \times \sin(2\pi \times 65 \times t) \\ & - 1.212 \times e^{-108.8t} \times \sin(2\pi \times 50 \times t) \\ & + 0.09204 \times e^{-365.6t}, \end{aligned} \tag{25}$$

$$\begin{aligned} v_q^+ - v_{q-\mathrm{pi}}^+ = {} & -18.6 \times e^{-155.8t} \times \sin(2\pi \times 38 \times t) \\ & + 16.88 \times e^{-144.4t} \times \sin(2\pi \times 40 \times t) \\ & + 1.163 \times e^{-101.3t} \times \sin(2\pi \times 25 \times t) \\ & + 0.05158 \times e^{-51.81t} \times \sin(2\pi \times 10 \times t). \end{aligned} \tag{26}$$

The circuit equation (17) and the inner loop control equation (18) are combined and reduced to the equation group shown in equation (24):

$$\begin{cases} v_d^+ - v_{d-\mathrm{pi}}^+ = -L\dfrac{d}{\mathrm{d}t}i_d^+ - \omega_{\mathrm{PLL}}\mathrm{L}i_q^+ - L\left[\cos\theta_{\mathrm{PLL}}f_1(t) + \sin\theta_{\mathrm{PLL}}f_2(t)\right] \\ + u_d^+ + \left[k_{\mathrm{ip}}(i_d^* - i_d^+) + k_{\mathrm{ii}}\displaystyle\int(i_d^* - i_d^+)\mathrm{d}t\right] + \omega_0\mathrm{L}i_q^+ - u_d^+, \\ v_q^+ - v_{q-\mathrm{pi}}^+ = -L\dfrac{d}{\mathrm{d}t}i_q^+ + \omega_{\mathrm{PLL}}\mathrm{L}i_d^+ - L\left[\sin\theta_{\mathrm{PLL}}f_1(t) - \cos\theta_{\mathrm{PLL}}f_2(t)\right] \\ + u_q^+ + \left[k_{\mathrm{ip}}\left(i_q^* - i_q^+\right) + k_{\mathrm{ii}}\displaystyle\int\left(i_q^* - i_q^+\right)\mathrm{d}t\right] - \omega_0\mathrm{L}i_d^+ - u_q^+. \end{cases} \tag{27}$$

Table 1: Simulation parameter.

ω_0	L	u_{dc}^*	Q^*
100π	0.000335 H	1.45 kV	0
k_{up}	k_{ui}	k_{ip}	k_{ii}
1	0.02	0.5	0.1

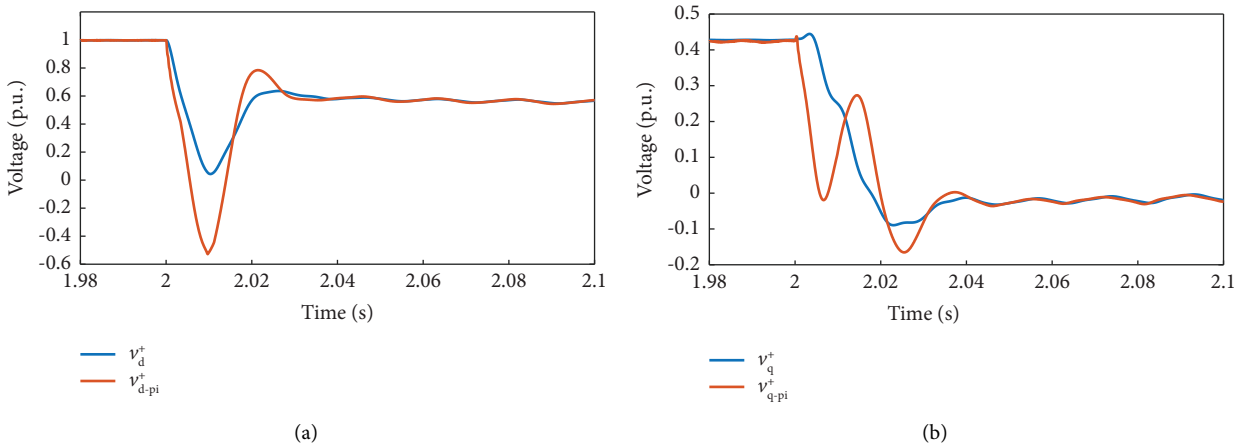

Figure 8: Output voltage of GSC in the dq-axis coordinate frame of positive sequence. (a) d-axis voltage and (b) q-axis voltage.

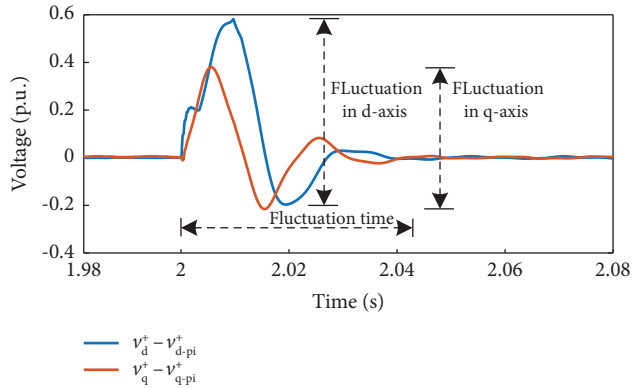

Figure 9: The difference between the calculated output voltage of GSC and the actual output voltage of GSC in the dq-axis coordinate frame of positive sequence.

In order to facilitate the solution, the integral terms are eliminated by taking the derivative of both sides of (34) and simplified into the nonhomogeneous second-order differential equations with variable coefficients about i_d^+ and i_q^+, which are shown in equation (25):

$$\begin{cases} \dfrac{d^2 i_d^+}{dt^2} = \dfrac{k_{ip}}{L}\dfrac{di_d^+}{dt} - (\omega_{PLL} - \omega_0)\dfrac{di_q^+}{dt} + \dfrac{k_{ii}}{L} i_d^+ - \dfrac{k_{ip}}{L}\dfrac{di_d^*}{dt} - \dfrac{k_{ii}}{L} i_d^* \\ + \dfrac{d}{dt}\left[\cos\theta_{PLL} f_1(t) + \sin\theta_{PLL} f_2(t) - \dfrac{1}{L}\left(v_d^+ - v_{d(pi)}^+\right)\right], \\ \dfrac{d^2 i_q^+}{dt^2} = \dfrac{k_{ip}}{L}\dfrac{di_q^+}{dt} + (\omega_{PLL} - \omega_0)\dfrac{di_d^+}{dt} + \dfrac{k_{ii}}{L} i_q^+ - \dfrac{k_{ip}}{L}\dfrac{di_q^*}{dt} - \dfrac{k_{ii}}{L} i_q^* \\ + \dfrac{d}{dt}\left[\sin\theta_{PLL} f_1(t) - \cos\theta_{PLL} f_2(t) - \dfrac{1}{L}\left(v_q^+ - v_{q(pi)}^+\right)\right]. \end{cases} \tag{28}$$

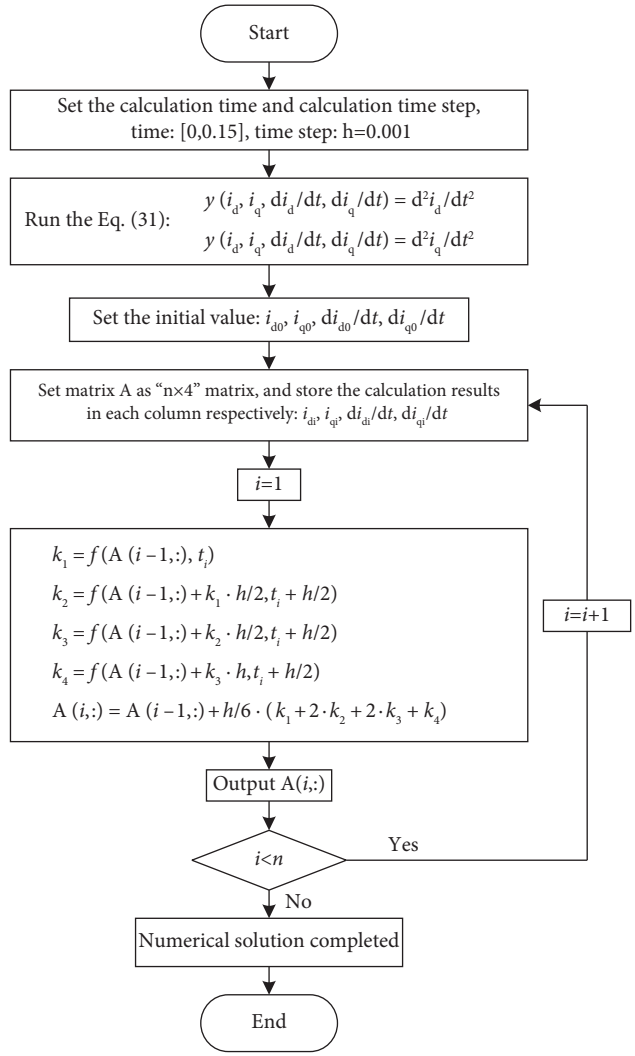

Figure 10: Numerical solution flowchart of the Runge–Kutta method.

Equations (25) and (26) are substituted into equation (28) as known quantities, and the fourth-order Runge–Kutta method is taken as an example to solve the dq-axis transient current of positive sequence i_d^+ and i_q^+. The specific solution process is shown in Figure 10 [30]:

In Figure 10, the basic idea of the Runge–Kutta method is to use a linear combination of function values at several points to replace the derivatives of the Taylor expansion, and then determine the coefficients according to the Taylor series expansion, so that we can not only avoid calculating higher derivatives but also improve the accuracy of the integral and the order of truncation error.

5.2. Solution and Simulation of Transient Current Verification under Different Voltage Drops. When the magnitude of positive sequence voltage at the PCC point u_{PCC} drops to about 7%, the comparisons between the calculation results and simulation values solved by (25) of the dq-axis transient currents of positive sequence i_d^+ and i_q^+ are shown in Figures 11(a) and 11(b):

It can be seen from Figures 11(a) and 11(b) that the errors between the dq-axis output currents of the positive sequence solved by (25) and the simulated currents are basically small. The simulation results show that the proposed method can effectively improve the accuracy of the research results of fault current transient characteristics by considering the positive and negative sequence decomposition. Through comparing the transient currents calculated by the existing research methods in Figures 5(a) and 5(b) with Figures 11(a) and 11(b), it can be learned that the positive and negative sequence decomposition link makes the transient currents have an obvious overshoot characteristic and a long duration time, which means the link has a great influence on the solution accuracy of the transient fault currents.

In order to verify whether the solution method proposed in Section 5.1 is suitable for different voltage drops, the magnitude of positive sequence voltage at the PCC point u_{PCC} is set to drop to 30% and 60%, respectively, when it reaches the steady state in the simulation. The waveforms of $v_d^+ - v_{d-\mathrm{pi}}^+$ and $v_q^+ - v_{q-\mathrm{pi}}^+$ are obtained as shown in Figures 12(a) and 12(b).

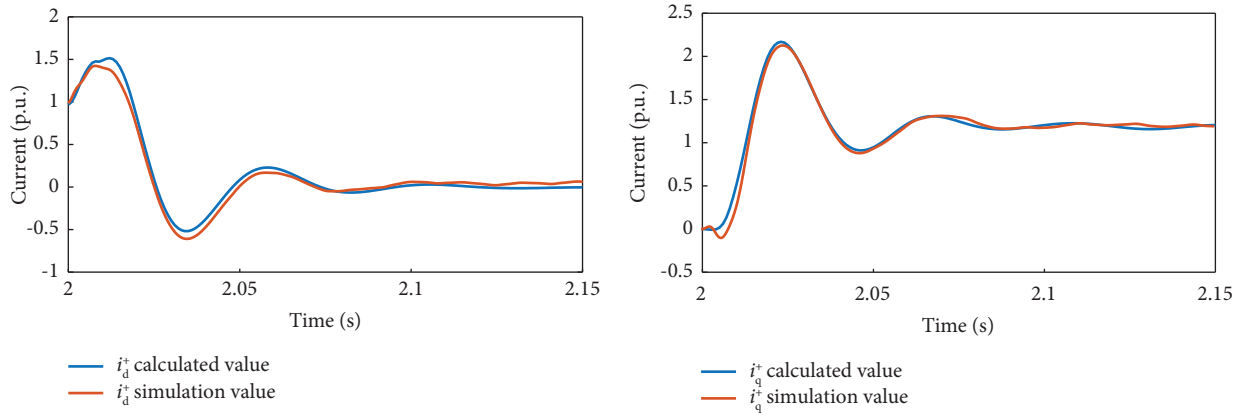

FIGURE 11: GSC output current of positive sequence when u_{PCC} drops to about 7%. (a) d-axis output current of positive sequence and (b) q-axis output current of positive sequence.

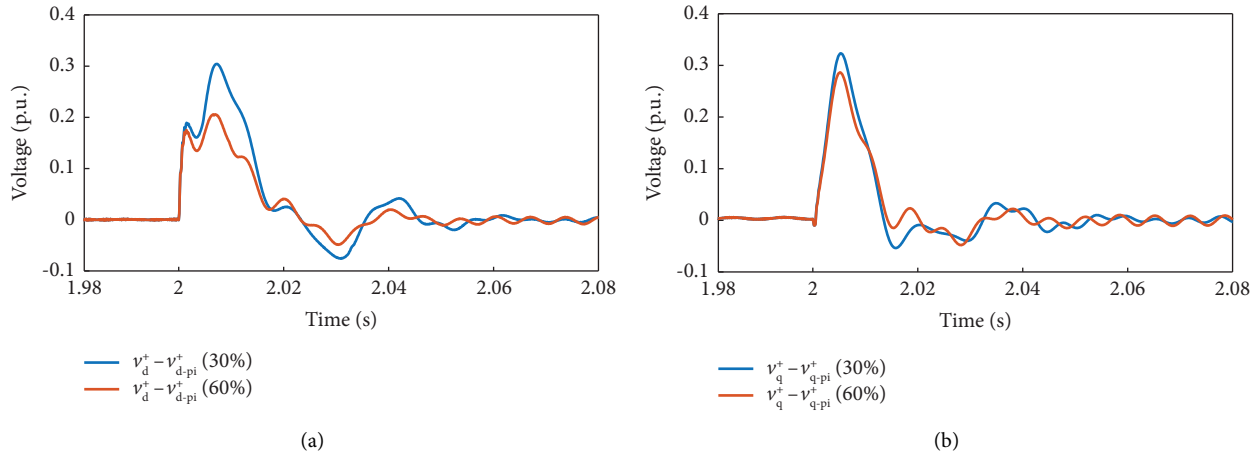

FIGURE 12: The difference between the calculated output voltage of GSC and the actual output voltage of GSC in the dq-axis coordinate frame of positive sequence. (a) The difference of the d-axis output voltage of the positive sequence and (b) the difference of the q-axis output voltage of the positive sequence.

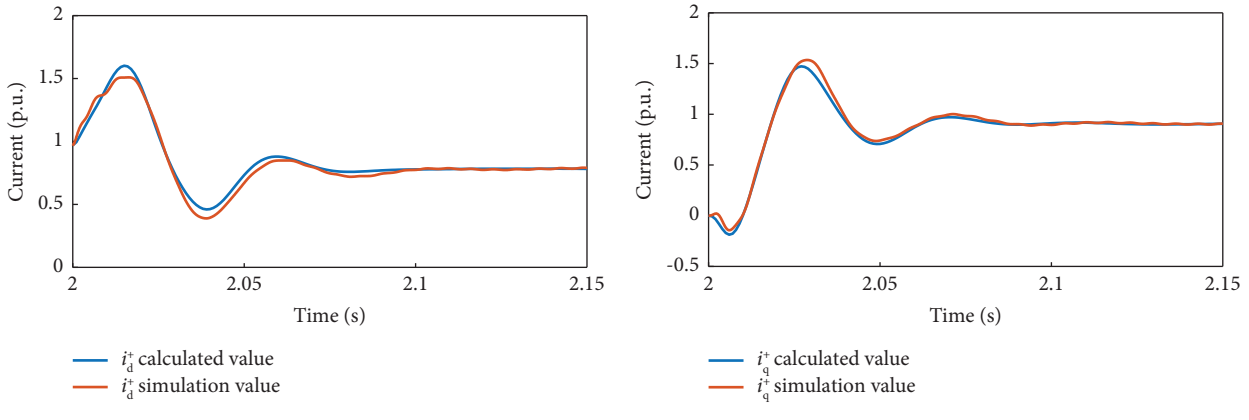

FIGURE 13: Continued.

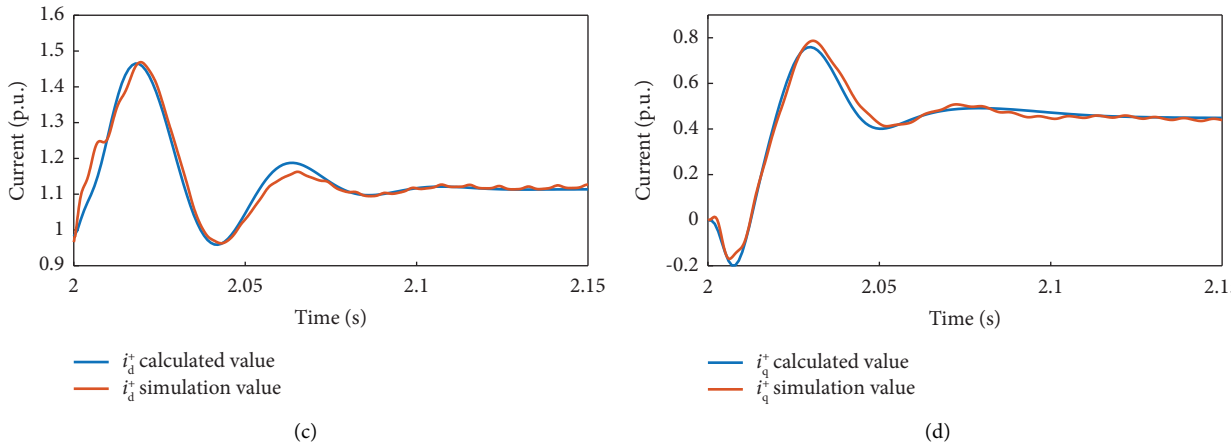

FIGURE 13: GSC output current of positive sequence. (a) i_d^+ when u_{PCC} drops to 30%, (b) i_q^+ when u_{PCC} drops to 30%, (c) i_d^+ when u_{PCC} drops to 60%, and (d) i_q^+ when u_{PCC} drops to 60%.

It can be learned from Figures 12(a) and 12(b) that the deeper the voltage drop of u_{PCC} is, the smaller the oscillation amplitudes of $v_d^+ - v_{d-pi}^+$ and $v_q^+ - v_{q-pi}^+$ are, but the oscillation trends of are similar.

The same fitting method as (22) and (23) is adopted to fit $v_d^+ - v_{d-pi}^+$ and $v_q^+ - v_{q-pi}^+$ when the magnitude of positive sequence voltage at the PCC point u_{PCC} reaches 30% and 60%, which are shown in (26) and (27):

$$\begin{aligned} v_d^+ - v_{d-pi}^+ = &-3.55 \times e^{-124.6t} \times \sin(2\pi \times 45 \times t) \\ &- 1.491 \times e^{-134.6t} \times \sin(2\pi \times 65 \times t) \\ &+ 5.173 \times e^{-157t} \times \sin(2\pi \times 50 \times t) \\ &+ 0.93 \times e^{-116.6t} \times \sin(2\pi \times 30 \times t), \end{aligned} \tag{29}$$

$$\begin{aligned} v_q^+ - v_{q-pi}^+ = &\ 0.006347 \times e^{-2.166t} \times \sin(2\pi \times 38 \times t) \\ &+ 1.467 \times e^{-202.9t} \times \sin(2\pi \times 40 \times t) \\ &+ 0.512 \times e^{-119.4t} \times \sin(2\pi \times 25 \times t) \\ &- 7.388 \times e^{-347.4t} \times \sin(2\pi \times 10 \times t). \end{aligned} \tag{30}$$

When the magnitude of u_{PCC} drops to about 60%, the expressions of $v_d^+ - v_{d-pi}^+$ and $v_q^+ - v_{q-pi}^+$ can be expressed as

$$\begin{aligned} v_d^+ - v_{d-pi}^+ = &-2.125 \times e^{-140.7t} \times \sin(2\pi \times 45 \times t) \\ &+ 1.029 \times e^{-1033t} \times \sin(2\pi \times 65 \times t) \\ &+ 1.129 \times e^{-108.7t} \times \sin(2\pi \times 50 \times t) \\ &+ 1.386 * e^{-142.2t} \times \sin(2\pi \times 30 \times t), \end{aligned} \tag{31}$$

$$\begin{aligned} v_q^+ - v_{q-pi}^+ = &-1.000e^{-224.4t} \times \sin(2\pi \times 38 \times t) \\ &+ 1.638 \times e^{-228.2t} \times \sin(2\pi \times 40 \times t) \\ &+ 0.3017 \times e^{-113.3t} \times \sin(2\pi \times 25 \times t) \\ &- 3.653 \times e^{-698t} \times \sin(2\pi \times 10 \times t). \end{aligned} \tag{32}$$

Equations (29) and (30), as well as equations (31) and (32), are substituted into equation (28) as known quantities, respectively, and the dq-axis transient currents of positive sequence i_d^+ and i_q^+ when voltage drop reaches 30% and 60% are calculated as shown in Figures 13(a)–13(d):

It can be learned from Figure 13 that the calculated current waveforms are basically consistent with the simulation waveforms, and the maximum error is less than 5%, which verifies the accuracy of the proposed analysis method of transient characteristics. The error between the calculation result and the simulation result is due to the approximate simplification of the inverter outlet voltage variation process in the calculation process to facilitate the solution, while the simulation variation process is more complex, and the accuracy of the calculation result is closely related to the simplified result. However, through comparison, it can be seen that the proposed method significantly improves the accuracy of the calculation results.

6. Conclusions

This paper focuses on the scenario of a voltage-symmetric drop at the PCC point caused by a three-phase fault of the permanent magnet direct-drive wind power system, proposing a fault analysis method for the output transient current of the wind farm, which takes into account the positive and negative sequence decomposition link of the control system because it is part of the control system and has an obvious transient response with a long duration. Then, it accurately depicts the transient characteristics of the fault current.

The computational principles proposed in this paper are also applicable to wind turbine control systems employing alternative positive-negative sequence decompositions. It is only necessary to substitute the equations corresponding to the DSOGI decomposition method used in this paper with those associated with other positive-negative sequence decomposition methods during the computation process.

The main results obtained are as follows:

(1) The transient change process of the electrical volume obtained after the positive and negative sequence decomposition is studied, and it is shown that the transient response of the positive and negative sequence decomposition leads to significant fluctuation and a long duration of the positive sequence component transient process. The reason why the coordinate transformation process of positive and negative sequence decomposition should be taken into account when establishing the calculation model of short-circuit current in the time domain is revealed.

(2) Based on the change characteristics of the positive and negative sequence decomposition, the *dq*-axis positive sequence circuit equation after the positive and negative sequence decomposition transformation is derived, and the characteristics of the circuit equation are analyzed. At the same time, the relationship between the output voltage of the converter in the circuit equation and the modulation signal of the converter output voltage in the control equation is derived. The analysis results show that the transient difference between the two makes it impossible to eliminate the converter output voltage as the intermediate variable when the control equation and the circuit equation are combined.

(3) A time-domain short-circuit current calculation model is formed by combining the *dq*-axis positive sequence circuit equation, the positive sequence control equation, the converter output voltage difference relation, and a short-circuit current transient characteristic analysis method for AC side faults of permanent magnet direct drive wind farm is proposed. The proposed method takes into account the influence of positive and negative sequence decomposition on the time domain short circuit current calculation model and is suitable for situations where the voltage of the PCC point has different sags. The calculated results accurately represent the characteristics of the *dq*-axis positive sequence current with an insurge current and a long transient duration.

Data Availability

No underlying data were collected or produced in this study.

Disclosure

This paper has been presented as a preprint according to the following link https://papers.ssrn.com/sol3/papers.cfm [31].

Conflicts of Interest

The authors declare that they have no conflicts of interest.

Acknowledgments

This work was supported in part by the Joint Funds of the National Natural Science Foundation of China under grant no. U2166205.

References

[1] Z. Hong, H. Su, H. Liu, and M. Zhao, "Research on key technologies and business models of low-carbon transformation of power industry under the 'double carbon' trend," in *2021 11th International Conference on Power and Energy Systems (ICPES)*, pp. 643–647, Shanghai, China, December 2021.

[2] W.-B. Mei, C.-Y. Hsu, and S.-J. Ou, "Research on the evaluation index system of the construction of communities suitable for aging by the fuzzy delphi method," *Environments*, vol. 7, pp. 92–110, 2020.

[3] J. Sun, M. Li, Z. Zhang et al., "Renewable energy transmission by HVDC across the continent: system challenges and opportunities," *CSEE Journal of Power and Energy Systems*, vol. 3, no. 4, pp. 353–364, 2017.

[4] Y. Guo, H. Geng, and G. Yang, "LVRT capability and improved control scheme of PMSG-based WECS during asymmetrical grid faults," in *IECON 2013-39th Annual Conference of the IEEE Industrial Electronics Society*, pp. 5294–5299, Vienna, Austria, November 2013.

[5] D. C. Meena and M. Singh, "Comparison of modern voltage parameter estimation techniques under various voltage conditions," in *2021 3rd International Conference on Advances in Computing, Communication Control and Networking (ICAC3N)*, pp. 1127–1132, Greater Noida, India, December 2021.

[6] J. Li-Jun, J. Miao-Miao, Y. Guang-Yao et al., "Unbalanced control of grid-side converter based on DSOGI-PLL," in *2015 IEEE 10th Conference on Industrial Electronics and Applications (ICIEA)*, pp. 1145–1149, June 2015.

[7] G. Tan, X. Zeng, Y. Zhang, J. Wei, Z. Chen, and X. Sun, "Model linearization analysis for three-phase unbalanced phase-locked loop techniques," in *2021 IEEE 4th International Electrical and Energy Conference (CIEEC)*, pp. 1–6, Wuhan, China, May 2021.

[8] U. Mumtahina, S. Alakahoon, and P. Wolfs, "A comparative study of phase locked loops for microgrid and storage converter applications," in *2021 IEEE PES Innovative Smart Grid Technologies-Asia (ISGT Asia)*, pp. 1–5, Brisbane, Australia, December 2021.

[9] A. C. Bingshuai, B. L. Chongjian, C. W. Chengsheng, D. D. Wei, and E. J. Jun, "An improved decoupled double synchronous reference frame phase locked loop and its application in grid connection system of permanent-magnet synchronous motor," in *2016 19th International Conference on Electrical Machines and Systems (ICEMS)*, pp. 1–6, Chiba, Japan, November 2016.

[10] Y. Wang, X. Chen, Y. Wang, and C. Gong, "Analysis of frequency characteristics of phase-locked loops and effects on stability of three-phase grid-connected inverter," *International Journal of Electrical Power and Energy Systems*, vol. 113, pp. 652–663, 2019.

[11] L. He, Z. Shuai, X. Zhang, X. Liu, Z. Li, and Z. J. Shen, "Transient characteristics of synchronverters subjected to asymmetric faults," *IEEE Transactions on Power Delivery*, vol. 34, no. 3, pp. 1171–1183, 2019.

[12] J. Li, H. Bi, C. Li, J. Li, D. Zeng, and G. Wang, "Analysis and calculation method for multiple faults in low-resistance grounded systems with inverter-interfaced distributed generators based on a PQ control strategy," *International Journal of Electrical Power and Energy Systems*, vol. 138, Article ID 107980, 2022.

[13] C. Zhang, J. Zeng, W. Zhao et al., "Fault characteristics of full power inverted sources and its short-circuit current calculation model," *Journal of Engineering*, vol. 2017, no. 13, pp. 2471–2476, 2017.

[14] X. Kuang, Y. Fang, H. Guan, J. Li, K. Jia, and T. Bi, "Full-time domain short circuit current calculation method suitable for power network with inverter-interfaced renewable energy source," *Electric Power Automation Equipment*, vol. 40, no. 5, pp. 113–120, 2020.

[15] Z. Chang, G. Song, X. Wang, S. Guo, W. Zhang, and X. Jin, "Analysis on asymmetric fault current of inverter interfaced distributed generator," in *2016 China International Conference on Electricity Distribution (CICED)*, pp. 1–6, Xi'an, China, August 2016.

[16] K. Jia, Q. Liu, B. Yang, L. Zheng, Y. Fang, and T. Bi, "Transient Fault current analysis of IIRESs considering controller saturation," *IEEE Transactions on Smart Grid*, vol. 13, no. 1, pp. 496–504, 2022.

[17] X. Wu, F. Zeng, X. Yuan et al., "SSO analysis of D-PMSGs-based wind farm considering the PLL," in *2019 IEEE 8th International Conference on Advanced Power System Automation and Protection (APAP)*, pp. 955–959, Xi'an, China, October 2019.

[18] K. Jia, L. Hou, Q. Liu, Y. Fang, L. Zheng, and T. Bi, "Analytical calculation of transient current from an inverter-interfaced renewable energy," *IEEE Transactions on Power Systems*, vol. 37, no. 2, pp. 1554–1563, 2022.

[19] Z. Yang, Q. Zhang, Z. Liu, and Z. Chen, "Fault current calculation for inverter-interfaced power sources considering saturation element," in *2021 IEEE 4th International Electrical and Energy Conference (CIEEC)*, pp. 1–5, Wuhan, China, May 2021.

[20] H. Zhao, Z. Shuai, J. Ge, A. Luo, W. Wu, and Z. J. Shen, "Asymmetrical fault current calculation method and influencing factors analysis of droop-controlled inverter," *CSEE Journal of Power and Energy Systems*, pp. 1–10, 2021.

[21] Q. Zhang, D. Liu, Z. Liu, and Z. Chen, "Fault modeling and analysis of grid-connected inverters with decoupled sequence control," *IEEE Transactions on Industrial Electronics*, vol. 69, no. 6, pp. 5782–5792, 2022.

[22] Q. Liu, K. Jia, B. Yang, L. Zheng, and T. Bi, "Fault analysis of inverter-interfaced RESs considering decoupled sequence control," *IEEE Transactions on Industrial Electronics*, vol. 70, no. 5, pp. 4820–4830, 2023.

[23] Y. Wang, C. Zhao, C. Guo, and A. U. Rehman, "Dynamics and small signal stability analysis of PMSG-based wind farm with an MMC-HVDC system," *CSEE Journal of Power and Energy Systems*, vol. 6, no. 1, pp. 226–235, 2020.

[24] P. Rodríguez, A. Luna, I. Candela, R. Mujal, R. Teodorescu, and F. Blaabjerg, "Multiresonant frequency-locked loop for grid synchronization of power converters under distorted grid conditions," *IEEE Transactions on Industrial Electronics*, vol. 58, no. 1, pp. 127–138, 2011.

[25] A. A. Nazib, D. G. Holmes, and B. P. McGrath, "Decoupled DSOGI-PLL for improved three phase grid synchronisation," in *2018 International Power Electronics Conference (IPEC-Niigata 2018-ECCE Asia)*, pp. 3670–3677, Niigata, Japan, May 2018.

[26] M. M. Kabsha and Z. H. Rather, "Advanced LVRT control scheme for offshore wind power plant," *IEEE Transactions on Power Delivery*, vol. 36, no. 6, pp. 3893–3902, 2021.

[27] J. Yao, J. Li, L. Guo, R. Liu, and D. Xu, "Coordinated control of a hybrid wind farm with PMSG and FSIG during asymmetrical grid fault," *International Journal of Electrical Power and Energy Systems*, vol. 95, pp. 287–300, 2018.

[28] K. Jia, C. Gu, Z. Xuan, L. Li, and Y. Lin, "Fault characteristics analysis and line protection design within a large-scale photovoltaic power plant," *IEEE Transactions on Smart Grid*, vol. 9, no. 5, pp. 4099–4108, 2018.

[29] Y. Fang, K. Jia, Z. Yang, Y. Li, and T. Bi, "Impact of inverter-interfaced renewable energy generators on distance protection and an improved scheme," *IEEE Transactions on Industrial Electronics*, vol. 66, no. 9, pp. 7078–7088, 2019.

[30] R. Lin, C. Wang, F. Liu, and Y. Xu, "A new numerical method of nonlinear equations by four order Runge-Kutta method," in *2010 IEEE International Conference on Industrial Engineering and Engineering Management*, pp. 1295–1299, Macao, China, December 2010.

[31] B. Li, Q. Zhong, W. Wen, B. Li, and X. Chen, "Study on transient characteristics of three-phase short-circuit fault current of offshore wind power delivery system including positive and negative sequence decomposition," *SSRN Electronic Journal*, 2022.